Available online at www.sciencedirect.com
SCIENCE DIRECT®
Journal of Nuclear Materials 349 (2006) 150–159
journal of nuclear materials
www.elsevier.com/locate/jnucmat

Derivation of analytical expressions for the network dislocation density, change in lattice parameter, and for the recrystallized grain size in nuclear fuels

J. Rest

Argonne National Laboratory, Energy Technology-212, 9700 S. Cass Avenue, Argonne, IL 60439, United States

Received 7 July 2005; accepted 7 October 2005

Abstract

At relatively high burn-up, both UO_2 and U–10Mo nuclear fuels undergo irradiation-induced recrystallization wherein grains of micron size transform to grains of submicron size. Previously, expressions have been derived for the initiation, and for the progression of recrystallization as a function of fission density, fission rate, fuel temperature, and as-fabricated grain size. Here, analytical expressions are derived for the network dislocation density, change in lattice parameter, and the size of the recrystallized grains. The basic premise of the theory presented in this work is that irradiation-induced recrystallization is driven by the behavior of interstitial loops. It is demonstrated that these phenomena can be simulated in both UO_2 and in U–*x*Mo with the same theory, albeit with various property differences. Results of the calculations are compared with available data.

1. Introduction

Irradiation-induced recrystallization appears to be a general phenomenon in that it has been observed to occur in a variety of nuclear fuel types [1], e.g. U–*x*Mo, UO_2, and U_3O_8. The recrystallization process results in sub-micron size grains that accelerate fission-gas swelling due to the combination of short diffusion distances, increased grain-boundary area per unit volume, and greater intergranular bubble growth rates as compared to that in the grain interior [2]. The initiation of recrystallization is to be distinguished from the subsequent progression and eventual consumption of the original fuel grain. Previously, an expression has been derived for the fission density at which irradiation-induced recrystallization is initiated that is athermal and weakly dependent on fission rate [3], and for the progression of recrystallization [4] that is independent of temperature and fission rate, linearly dependent on the fission density, and inversely proportional to the cube of the as-fabricated grain size.

The driving force for recrystallization is the production of point defects and interstitial loops due to irradiation. In this work it is assumed that due to recombination and to the generation of interstitial loops, the point-defect densities remain relatively

E-mail address: jrest@anl.gov

0022-3115/$ - see front matter © 2005 Elsevier B.V. All rights reserved.
doi:10.1016/j.jnucmat.2005.10.007

low as the irradiation proceeds, and thus, only the effect of interstitial loops is considered. The continued generation of interstitial loops induces internal stresses in the material that leads to strain in the form of lattice displacement. The initiation of recrystallization in U–10Mo has been observed to occur predominately along the pre-existing grain boundaries [1]. The surfaces of preexisting voids can also act as nucleation sites for recrystallization, but will not be considered in this work. Subsequently, the recrystallization front moves toward the grain center eventually consuming the entire grain. Thus, the volume fraction of recrystallized material is a function of irradiation time as well as the initial grain size. As gas-bubble swelling is higher in the recrystallized material than in the unrecrystallized fuel, the swelling due to fission gas is a function of the recrystallization kinetics.

In Section 2 models for the initiation and progression of irradiation-induced recrystallization are reviewed. Section 3 presents a theory for the size of the recrystallized grains. In Section 4, calculations are compared to data for the dislocation density and change in lattice displacement in UO_2 as a function of burn-up.

In Section 5, calculations are compared to available data for the recrystallized grain-size distribution in UO_2 and in U–10Mo. Finally, conclusions are presented in Section 6.

2. Review of model for initiation and progression of irradiation-induced recrystallization

The recrystallization nuclei are taken as the triple points of an evolving cellular dislocation network. The relevant kinetics are those of interstitial-loop formation and agglomeration that lead to the formation of a dislocation network in an environment of precipitate pinning [3,5]. The trigger point for irradiation-induced recrystallization is defined as the point where the kinetically derived concentration of viable nuclei becomes equal to the equilibrium number of nuclei determined from thermodynamic considerations.

The critical fission density F_{dx} at which recrystallization will occur is given by [3]

$$F_{dx} = \left(\frac{\alpha_p \rho_d(T)}{\phi\gamma}\right)^{4/5} \left(\frac{2\lambda}{3 b_v B_0 \beta}\right)^{1/5} \times \frac{f(v)^{6/5} \exp\left[4(\varepsilon_v/2 - \varepsilon_i)/15kT\right]}{\pi^{9/5}(C_A C_\rho)^{12/5}}, \quad (1)$$

where $\rho_d(T)$ is the temperature-dependent dislocation density, $\phi\gamma/\alpha_p$ is a factor composed of terms related to the production of precipitates and sub-grain growth in the presence of precipitates, b_v is the van der Waals constant, λ is the atom knock-on distance, $f(v) = (1 - v/2)/(1 - v)$, v is Poisson's ratio, C_A is three for cubic cells, C_ρ is within a factor of unity, β is the number of gas atoms produced per fission, ε_i and ε_v are the interstitial and vacancy migration enthalpies, respectively, and where, at the relatively low temperatures T where irradiation-induced recrystallization occurs, the gas atom diffusivity is athermal and can be expressed as $D_g = B_0\dot{f}$, where B_0 is a constant of proportionality (10^{-39} m^{-3}) and $\dot{f}$ is the fission rate.[1]

The fission density at which recrystallization is predicted to initiate as given by Eq. (2) is athermal and very weakly dependent on fission rate. As such, F_{dx} is independent of ε_v and ε_i and depends primarily on the collision related parameters λ, D_g and $\alpha_p/\phi\gamma$. Substituting nominal values of the parameters (e.g. corresponding to UO_2 [3]) in Eq. (1) leads to the simplified expression for F_{dx} (m^{-3}):

$$F_{dx} = 4 \times 10^{24} (\dot{f})^{2/15}, \quad (2a)$$

$$F_{dx} = 6 \times 10^{24} (\dot{f})^{2/15}, \quad (2b)$$

where Eq. (2a) corresponds to UO_2 and Eq. (2b) to U–10Mo.

A model for the progression of recrystallization as a function of burn-up has been developed [4] based on the following assumptions: (1) recrystallization initiates at preexisting grain boundaries; (2) annuli located initially adjacent to the original grain boundary, transform to defect free regions via the creation of the new recrystallized surface when the volumetric strain energy exceeds that necessary to create the new surface; and (3) the rate at which the defect front moves through the newly created defect free annulus is proportional to the strain rate, which, in analogy with fission-induced creep, is proportional to stress and fission rate. The microscopic stress is a function of the lattice displacement, which is related to the generation rate of interstitial loops.

The volume fraction of recrystallized fuel as a function of fission density is given by

[1] Eqs. (1) and (2a) are the corrected versions of Eqs. (33) and (34) in Ref. [3].

$$V_r = 1 - \left[1 - \frac{96\gamma_s B_2 (F_d - F_{dx})}{d_g C_A C_\rho}\sqrt{\frac{f(v)}{2\pi}}\right]^3, \quad (3)$$

where B_2 is a parameter in the expression for fission-induced microscopic creep, i.e. $\dot{\varepsilon} = B_2 \dot{f}\sigma$, and the stress is a function of the lattice displacement, $\sigma = E\Delta a/a_0$, where E is the bulk modulus of the material. The volume fraction of recrystallized fuel as given by Eq. (3) does not depend on any details of the evolving defect structure in the material, but depends only on the parameter B_2, the as fabricated grain size d_g, and on the fission density.

3. Theory for the size of the recrystallized grains

When dislocation loops are large enough relative to the inter-atomic distances but small relative to the crystal dimensions, they produce a measurable lattice distortion that can be expressed as [6]

$$\Delta a(t)/a_0 = \pi b_v n_l(t) d_l^2(t)/12, \quad (4)$$

where $n_l(t)$ is the volumetric loop density and $d_l(t)$ is the loop diameter. For UO_2, the Burgers vector b_v is parallel to the [1 1 0] direction, with $b_v = (a/2)2^{1/2}$, and where a is the lattice parameter.

The increase in the lattice parameter is the driving force for irradiation-induced recrystallization. The recrystallized grain size can be calculated by equating the total energy change during the transition with the energy required to create the new surfaces. In addition to the volumetric strain energy, there is an entropy increase in going from the untransformed to the transformed state that should, in principle, be taking into account. The total free energy change upon recrystallization consists of the decrease in volumetric stain energy ΔU and the increase in the volumetric configurational entropy ΔS. Thus, the diameter of the newly recrystallized grains d_g^x can be calculated by equating the total free energy change $\Delta U + T\Delta S$ with the energy required to create the new surfaces, i.e. if the recrystallized grain shape is taken to be spherical, then

$$\frac{4\pi}{3}\left(\frac{d_g^x}{2}\right)^3 (\Delta U + T\Delta S) = \frac{3\gamma_{gb}}{d_g^x}\frac{4\pi}{3}\left(\frac{d_g^x}{2}\right)^3 \quad (5)$$

and solving for d_g^x

$$d_g^x = \frac{3\gamma_{gb}}{\Delta U + T\Delta S}, \quad (6)$$

where γ_{gb} is the energy per unit area of the sub-grain boundary and the volumetric stain energy is given by

$$\Delta U = \frac{1}{2}\left(\frac{\Delta a}{a_0}\right)^2 E, \quad (7)$$

where E is the elastic modulus of the material.

Recrystallization occurs after the cellular dislocation network has formed. Thus, from Eq. (4)

$$\Delta a/a_0 = \frac{b_v C_A C_\rho}{12}\sqrt{\frac{\pi}{f(v)}}\rho_N^{1/2}, \quad (8)$$

where

$$\rho_N = \pi n_l d_l \quad (9)$$

i.e. the interstitial loop line length is conserved, and the lowest energy configuration is a cellular dislocation network with cell size given by [7]

$$d_l = C_A C_\rho \sqrt{\frac{\pi}{\rho_N f(v)}}. \quad (10)$$

Eq. (8) is to be understood in the context of a relationship between the cellular network dislocation density ρ_N and the interstitial loop density n_l, i.e. it is the loops that are causing the lattice displacement and not the dislocations that make up the cellular dislocation structure. This relationship between ρ_N and n_l will be treated explicitly in the next section.

Substituting Eqs. (7)–(9) into Eq. (6) results in the following expression for d_g^x:

$$d_g^x = \frac{(12)^3\gamma_s f(v)}{\sqrt{2}\pi b_v E (C_A C_\rho)^2 \rho^{1/2}(t_x) + 2\sqrt{2}(12)^2 b_v^{-1} f(v) T\Delta S \rho^{-1/2}(t_x)}, \quad (11)$$

where

$$\gamma_{gb} = 2\gamma_s \mathrm{Tan}^{-1}\left(b_v\sqrt{\rho_N/2}\right) \approx 2\gamma_s b_v\sqrt{\rho_N/2}, \quad (12)$$

and where γ_s is the surface energy, and b_v is the magnitude of the burgers vector.

In Eq. (11), t_x is the time at which irradiation-induced recrystallization occurs, i.e. from Eq. (2)

$$t_x = 4 \times 10^{24}/(\dot{f})^{13/15}, \quad (13a)$$

$$t_x = 6 \times 10^{24}/(\dot{f})^{13/15}, \quad (13b)$$

where Eq. (13a) corresponds to UO_2 and Eq. (13b) to U–10Mo.

The recrystallized grain size as given by Eq. (11) depends on the ratio of the materials surface energy to the elastic modulus, the network dislocation density, and the change in configurational entropy. The calculation of the cellular network dislocation density is presented in the next section.

4. Calculation of the cellular network dislocation density and change in lattice parameter

In Section 2 the progression of recrystallization was described in terms of annuli located initially adjacent to the original grain boundary that transform to defect free regions via the creation of the new recrystallized surface when the volumetric strain energy exceeds that necessary to create the new surface [4]. The defects in the region interior to the defect-free annulus consist of a cellular dislocation network. The model for the time-dependent cellular network dislocation density ρ_N is given by the following equations

$$\frac{d\rho_N}{dt} = \pi v_l n_l - \frac{4v_l}{d_g}\rho_N - \frac{v_l(f(v)/\pi)^{1/2}}{C_A C_\rho}\rho_N^{3/2}, \tag{14}$$

$$\frac{dn_l}{dt} = \frac{\sqrt{2}}{2} D_i c_i^2/\Omega^{5/3} - v_l n_l/d_l, \tag{15}$$

$$v_l = \frac{2Z_{iv}}{b_v} D_i c_i. \tag{16}$$

In Eqs. (14)–(16) n_l and d_l are the interstitial loop density and diameter, respectively, v_l is the interstitial loop climb controlled glide velocity, D_i and c_i are the interstitial diffusivity and concentration, respectively, Z_{iv} is the relative bias between interstitials and vacancies, and Ω is the atomic volume. In Eq. (15), the first term on the right hand side represents the nucleation rate of interstitial loops due to di-interstitials; and the second term is the loss of loops to the dislocation network. In Eq. (14), the first term on the right hand side represents dislocation line length creation due to accumulation of interstitial loops, the second term represents the loss of line length due to capture of dislocations by the grain boundary (for the fabrication and irradiation conditions explored in this paper, this term can be neglected), and the third term represents loss of line length due to self annihilation via correlated movement of adjacent edge dislocations [8]. The dislocation is generally a mixture of screw and edge components in the shape of a loop. Mixed dislocations are characterized by a single Burgers vector. As the important deformation properties of the material, such as creep rate and the yield stress are controlled primarily by the edge components of the dislocation loop [9], the screw component of the loop has been ignored for the sake of simplicity. The form of the third term in Eq. (14) can also be deduced from the combined requirements imposed by Eqs. (9) and (10), i.e. that the dislocation line length is generated from interstitial loops and that the underlying structure is that of a cellular dislocation network. Eqs. (9) and (10) can be combined to yield: $n_l = \rho_N^{3/2}(f(v)/\pi)^{1/2}/\pi C_A C_\rho$. An identical expression to this one is also obtained from the steady-state solution of Eq. (14) in the limit of large grain size.

Based on more detailed analysis [10], the component of the interstitial loop density that is generated from defect nucleation and diffusion reaches steady state relatively early in the irradiation, i.e. from Eqs. (10) and (15) with $dn_l/dt = 0$

$$\frac{\sqrt{2}}{2} D_i c_i^2/\Omega^{5/3} - \frac{\pi v_l n_l^2}{\rho_N} = 0. \tag{17}$$

Using Eq. (16) in Eq. (17) and solving for the interstitial loop density yields

$$n_l = \left[\frac{\sqrt{2} b_v}{4\pi Z_{iv}\Omega^{5/3}} c_i \rho_N\right]^{1/2}. \tag{18}$$

Eq. (18) establishes a connection between the network dislocation density ρ_N and the interstitial loop density n_l , i.e. at any given time within the steady state regime there is a balance between n_l and ρ_N specified by Eq. (18).

Using Eq. (18), the equation for ρ_N, Eq. (14), is now solved analytically to obtain

$$\rho_N(t) = \frac{c_1}{c_2}\left[\frac{1 - e^{\sqrt{c_1 c_2}t}}{1 + e^{\sqrt{c_1 c_2}t}}\right]^2, \tag{19}$$

where

$$c_1 = \left[\pi v_l \frac{\sqrt{2}}{2} D_i c_i^2/\Omega^{5/3}\right]^{1/2} \tag{20}$$

and

$$c_2 = \frac{v_l(f(v)/\pi)^{1/2}}{C_A C_\rho}, \tag{21}$$

where the steady-state concentration of interstitials is given by

$$c_i = \frac{1}{D_i}\left(\frac{\Omega D_v K}{4\pi r_{iv}}\right)^{1/2} \tag{22}$$

and K is the damage rate in atomic displacements per atom ($K \approx \dot{f}/10^{23}$), D_v the vacancy diffusivity, and r_{iv} the defect recombination distance. The temperature dependence of c_i in Eq. (22) is contained in the interstitial and vacancy diffusivities. In

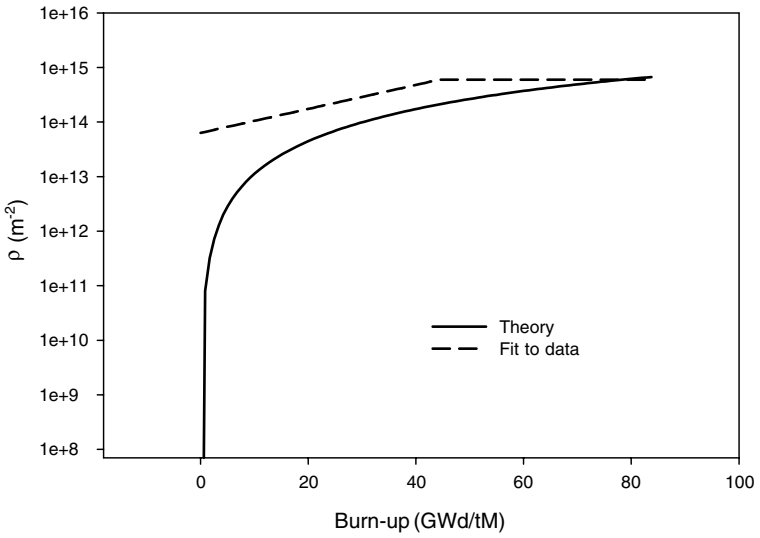

Fig. 1. Calculated dislocation density for $T = 953$ K as a function of burn-up. Also shown is a fit to measured dislocation density from Ref. [13].

general, these diffusivities are expressed as $D_i = D_i^0 \exp(-\varepsilon_i/kT)$ and $D_v = D_v^0 \exp(-\varepsilon_v/kT)$.

Fig. 1 shows the cellular network dislocation density at $T = 953$ K calculated with Eqs. (16), (19)–(22) as a function of burn-up. The calculations incorporated the properties listed in Table 1. Also shown is a fit to the measured dislocation density from Ref. [13]. The calculations shown in Fig. 1 tend to under-predict the data in the lower burn-up range. This result is consistent with the steady-state assumption invoked for the interstitial loop density given by Eq. (18). As shown in Fig. 1, the calculated network dislocation density approaches the data as the fuel local burn-up approaches 80 GWd/tM. The calculated values for the dislocation density exceed the data trend line at high local burn-up (>80 GWd/tM). The reason for this is, presumably, as mentioned by the authors of Ref. [13], the inaccuracy of counting highly tangled configurations of dislocations. In any event, it is the evolution of the network dislocation density in the fuel burn-up regime characterized by the approach to recrystallization that is critical to the calculation of the change in lattice parameter as given by Eq. (8), and the recrystallized grain size as given by Eq. (11). As shown in Fig. 1, the calculated values follow the trend of the data in this regime.

Table 1
Values of various parameters used in the calculation for UO_2

Parameter	Value	Reference
D_i^0	$5\ m^2\ s^{-1}$	[10]
D_v^0	$75\ m^2\ s^{-1}$	[10]
ε_i	0.6 eV	[10]
ε_v	2.4 eV	[11]
r_{iv}	82.5 Å	[10]
Z_{iv}	5×10^{-4}	[10]
a	5.47 Å (UO_2)	[9]
b_v	$\sqrt{2}a/2$	[9]
E	$2 \times 10^{11}\,(1 - 1.09154 \times 10^{-4}\,T)$ Nm^{-2}, (UO_2, 0.95 TD)	[12]
γ_s	$1\ Jm^{-2}$	[9]
B_2	$2 \times 10^{-34}\ m^5\ N^{-1}$	[4]
ΔS	$2 \times 10^{-6}\ Jm^{-3}\ K^{-1}$	This work

Fig. 2 shows the change in UO_2 lattice parameter at $T = 923$K calculated with Eqs. 3, 8 and (19)–(22) vs. burn-up relative to a fit to the experimental data [14]. In Fig. 2, the initiation of recrystallization, given by Eq. (2a), occurs at the peak of the calculated curve, i.e. at $\Delta a(t)/a_0 \approx 10^{-3}$. Subsequently, $\Delta a(t)/a_0$ decreases due to the progression of recrystallization, as given by Eq. (3). As pointed out by Spino et al. [14], there are many other factors aside from interstitial loops that give rise to a change in lattice parameter, e.g. the lattice parameter is affected by fission product concentrations, alpha damage, etc. However, for the lattice-constant measurements in Ref. [14], it was determined that the chemical effects in the rim were of second order in importance.

As shown in Fig. 2, the calculated change in $\Delta a(t)/a_0$ follows the trend of the data. As such, it appears that lattice distortion induced by the

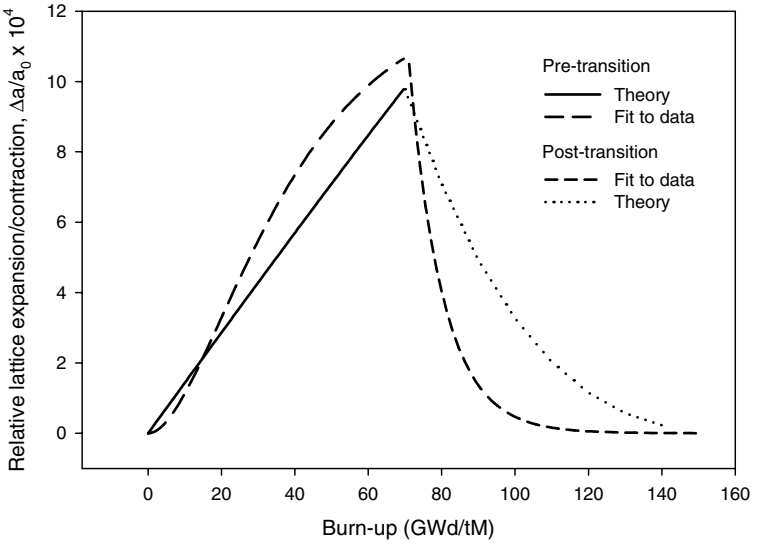

Fig. 2. Calculated change in UO_2 lattice parameter at $T = 923$ K vs. burn-up relative to fit to experimental data [14].

presence of interstitial loops provides a relatively large contribution.

5. Calculation of recrystallized grain size

Using Eqs. 11, (13), (19)–(22), and the properties listed in Table 1, the average recrystallized grain size can now be calculated. Fig. 3 shows the calculated recrystallized grain size in UO_2 at $T = 923$ K as a function of the average fission rate $\dot{f}$. The recrystallized grain size is calculated at the time of recrystallization. Grain growth subsequent to the recrystallization event is not considered here. As is evident from Fig. 3, the calculated recrystallized grain size increases as the average fission rate in the fuel increases. Fig. 4 shows the calculated recrystallized grain size in UO_2 for $\dot{f} = 2 \times 10^{19}\ \mathrm{m^{-3}\,s^{-1}}$ as a function of the fuel temperature for various values of the volumetric configurational entropy change ΔS upon recrystallization. As demonstrated in Fig. 4, for fuel temperatures >800 K the calculated recrystallized grain size decreases as the fuel temperature increases. For fuel temperatures <850 K and for relatively large values of $T\Delta S$ that

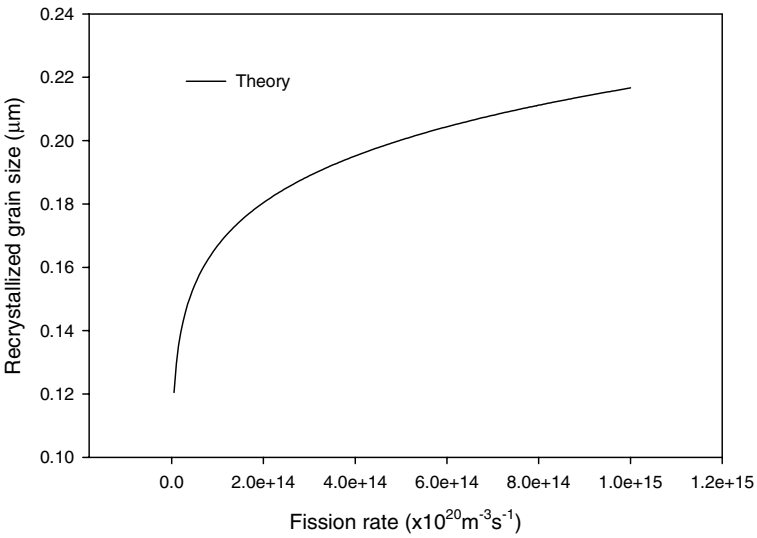

Fig. 3. Calculated recrystallized grain size in UO_2 at $T = 923$ K as a function of the average fission rate $\dot{f}$.

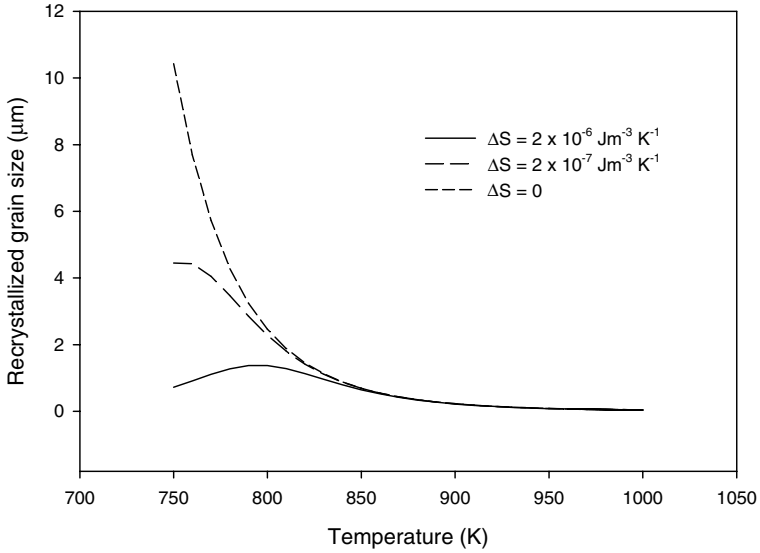

Fig. 4. Calculated recrystallized grain size in UO_2 for $\dot{f} = 2 \times 10^{19}\ m^{-3}\ s^{-1}$ as a function of the fuel temperature for various values of the volumetric configurational entropy change ΔS upon recrystallization.

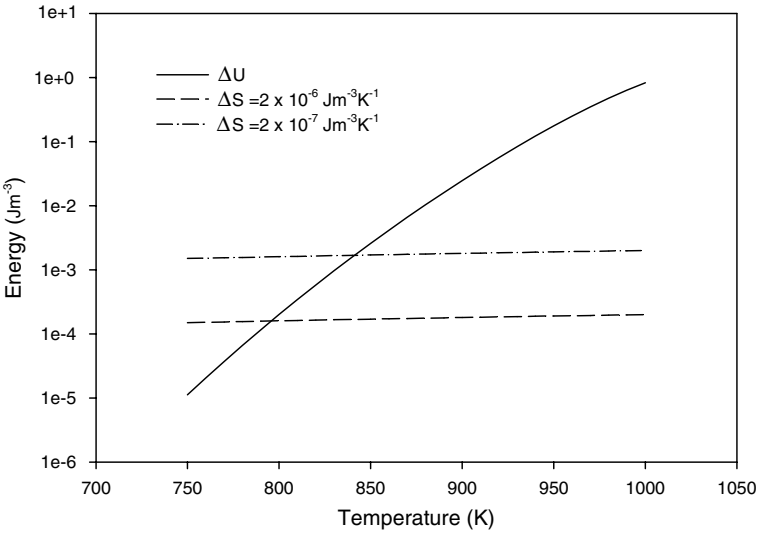

Fig. 5. Calculated volumetric strain energy in UO_2 for $\dot{f} = 2 \times 10^{19}\ m^{-3}\ s^{-1}$ as a function of the fuel temperature compared with the various values for the assumed volumetric configurational entropy change upon recrystallization.

are on the order of ΔU ($\approx 10^{-4} - 10^{-3}\ Jm^{-3}$ as shown in Fig. 5) the second term in the denominator of Eq. (11) will offset the first term (which decreases as the temperature decreases) such that the recrystallized grain size calculated with Eq. (11) reaches a maximum, and then subsequently decreases as the temperature is further lowered.

The effect of including the entropy term in Eq. (11) is also demonstrated in Fig. 5 which shows the calculated volumetric strain energy ΔU in UO_2 for $\dot{f} = 2 \times 10^{19}\ m^{-3}\ s^{-1}$ as a function of the fuel temperature compared with several values for the volumetric configurational entropy change ΔS upon recrystallization. As shown in Fig. 5, ΔU becomes comparable to $T\Delta S$ at fuel temperatures <850 K.

Comparing Figs. 3 and 4, it is clearly seen that the effect of temperature on recrystallized grain size is much stronger than that of fission rate. Although this

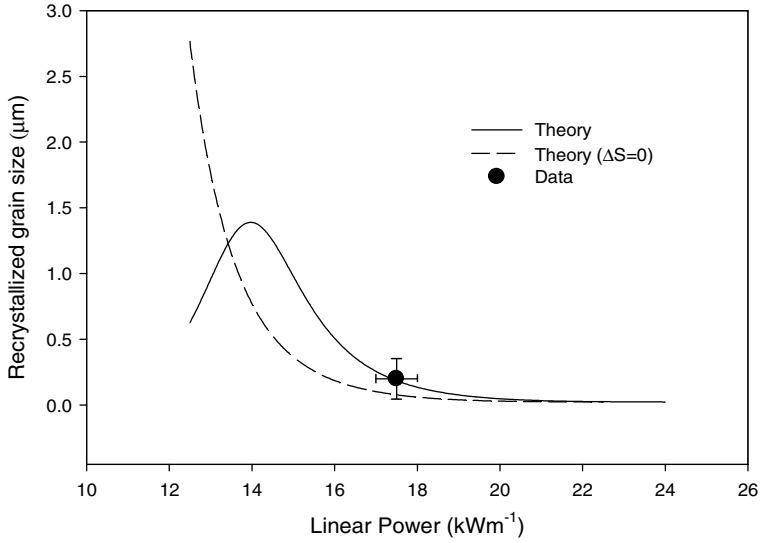

Fig. 6. Calculated average recrystallized grain size in UO_2 as a function of linear power compared with measured values [19].

result is at odds with some reported results [15,16], it is consistent with new experimental evidence that the recrystallized grain-size distribution is temperature dependent [17]. Again, care must be taken in comparing the results of the calculations for recrystallized grain size at the moment of recrystallization with data on grain size distributions measured at local fuel burn-ups far beyond the recrystallization burn-up.

Fig. 6 shows the calculated recrystallized grain size in UO_2 as a function of average linear power. The fuel temperature used to calculate the recrystallized grain size in Fig. 6 was estimated based on the relationship between linear power and fuel temperature developed by Bagger et al. (e.g. see Eq. (12) in Ref. [18]). Also shown in Fig. 6 is the average grain size in the recrystallized region of the fuel from the work of Spino et al. [19]. The theoretical results shown in Fig. 6 indicate that there is a relatively small change in the grain size for average linear power >18 kW/m. Between 12 and 18 kW/m the calculated grain size is bell shaped with a maximum occurring at about 14 kW/m.

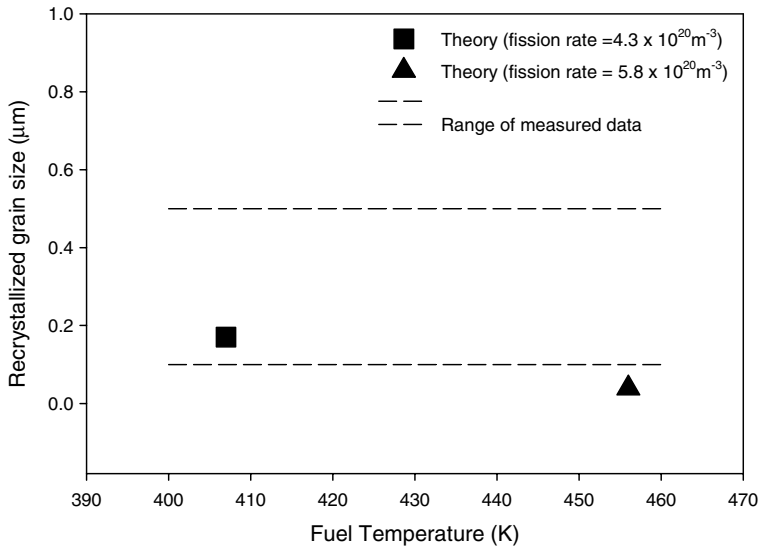

Fig. 7. Calculated average recrystallized grain size in U–10Mo as a function of fuel temperature compared with the trend of measured values [21].

Table 2
Values of various parameters used in the calculation of U–10Mo

Parameter	Value	Reference
ε_i	$0.6 * \frac{T_M^{U-10Mo}}{T_M^{UO_2}}$ eV	This work
ε_v	$2.4 * \frac{T_M^{U-10Mo}}{T_M^{UO_2}}$ eV	This work
D_i^0	$\left(\frac{a(U-10Mo)}{a(UO_2)}\right)^2 D_i^0(UO_2)$	This work
D_v^0	$\left(\frac{a(U-10Mo)}{a(UO_2)}\right)^2 D_v^0(UO_2)$	This work
Z_{iv}	$10Z_{iv}(UO_2)$	This work
a	3.42Å	[20]
b_v	1.5Å	[20]
E	8.3×10^{10} Nm^{-2}	[20]
T_M^{U-10Mo}	1408 K	[20]
$T_M^{UO_2}$	3123 K	[9]

Only the properties that differ from those in Table 1 are listed.

Also shown in Fig. 6 are the results of calculations made without the effect of including the entropy term (i.e.$\Delta S = 0$) in Eq. (5). As is evident in Fig. 6, not including this mechanism results in a relatively strong dependence of the recrystallized grain size on the linear power for values of the linear power <15 kW/m.

Unfortunately, for U–xMo there is a much greater uncertainty in the properties (e.g. those in Table 1) than for UO_2. Fig. 7 shows the calculated average recrystallized grain size in U–10Mo made using the properties listed in Table 2 as a function of fuel temperature compared with the trend of measured values [21]. Only the properties that differ from those in Table 1 are listed in Table 2. The results shown in Fig. 7 indicate that the theoretical calculation for the recrystallized grain size in U–10Mo is order of magnitude comparable with the data.

6. Discussion and conclusions

The basic premise of the theory proposed in this work is that irradiation-induced recrystallization is driven by the behavior of the interstitial loops in the material. Interstitial loops interact and lead to the formation of dislocations and a cellular dislocation structure. Evolving subgrains are characterized by relatively low angle and may remain thus until recrystallization is initiated which leads to the formation of nanometer size grains having large angle boundaries.

However, Ray et al. [15] report that the grain boundary angles are exclusively low angel (<5°) in the rim region. This observation supports the microstructural evolution through polygonization and is inconsistent with recrystallization even though the local burn-up of the samples exceeded 200 GWd/tM. Similarly, Sonada et al. [22] report a low-angle subgrain structure in 90 GWd/tM samples and, thus, support polygonization as the prime mechanism for grain refinement.

On the other hand, Thomas et al. [23] and Nogita et al. [24] report a mixture of low and high angle submicron grains in the rim region at ≈100 GWd/tM. These observations support the further evolution of a cellular dislocation microstructure into low-angle subgrains and recrystallized grains.

The theory described here sides with the latter viewpoint that not only polygonization, but recrystallization is occurring in these materials. Recrystallization provides a mechanism for the reduction in the lattice displacement as shown in Fig. 2. In addition, recrystallization provides a mechanism for the lowering of the free energy, consisting of decreasing volumetric strain energy and increasing entropy, in exchange for the creation of new surfaces associated with the newly formed recrystallized grains. Indeed, this scenario is consistent with observations of relatively defect free interiors of the recrystallized grains in UO_2 [13].

The entropy term in Eq. (11) is responsible for flattening out the calculated recrystallized UO_2 grain size vs. temperature curve for fuel temperatures <800 K (Figs. 4 and 5). It is interesting to note that this term has a negligible effect on the calculated recrystallized grain size for the U–10Mo irradiation conditions shown in Fig. 7. On the other hand, the calculated dislocation density given by Eq. (19) continues to decrease as the temperature decreases. This result is in apparent contradiction to some observations that the dislocation density in UO_2 is relatively constant across the fuel radius [25]. However in a later publication, Ray et al. found about 1 order of magnitude difference in the dislocation density and about four orders of magnitude difference between dislocation loop densities measured in the rim and in the center of the pellet irradiated to 74 GWd/tM [15].

This work has, for the most part, focused on the point at which recrystallization is initiated. For this reason, the effects of porosity development and xenon depletion have been ignored. In general, the majority of the porosity development and xenon depletion observed in UO_2 fuels occurs subsequent to the initiation of recrystallization. Porosity development and

xenon depletion as a function of burn-up have been treated in other publications [4,26].

The theory presented in this work is novel in the sense that a reasonably complete picture consisting of the initiation and progression of recrystallization and the determination of the recrystallized grain size is provided by analytically derived expressions. In addition, analytical expressions are provided for the time-dependent network dislocation density and change in lattice parameter.

It has been demonstrated that these phenomena can be simulated in both UO_2 and in U–xMo with the same theory, albeit with various property differences. That this is possible reflects the likelihood that the defect behavior in both materials in the temperature regime where recrystallization is observed to occur is characterized by the uranium interstitial, by the associated formation of interstitial loops, and by athermal diffusion of gas atoms. Results of the calculations are consistent with the trends of the available data.

Acknowledgements

Work supported by US Department of Energy, Office of Arms Control and Nonproliferation, National Nuclear Security Administration (NNSA), under Contract W-31-109-ENG-38.

References

[1] J. Rest, G.L. Hofman, in: Proceedings of the Materials Research Society Meeting, Symposium R, Boston, MA, November 2000.
[2] J. Rest, J. Nucl. Mater. 321 (2003) 305.
[3] J. Rest, J. Nucl. Mater. 326 (2004) 175.
[4] J. Rest, J. Nucl. Mater. 346 (2005) 226.
[5] J. Rest, G.L. Hofman, J. Nucl. Mater. 210 (1994) 187.
[6] M.A. Krivoglaz, X-Ray and Neutron Diffraction in Nonideal Crystals, Springer, Berlin, 1995 (Chapters 3 and 4).
[7] N. Hanson, D. Kuhlmann-Wilsdorf, Mater. Sci. Eng. 81 (1986) 141.
[8] F.A. Garner, W.G. Wolfer, in: H.R. Brager, J.S. Perrin (Eds.), Effects of Radiation on Materials: Eleventh Conference, ASTM STP, 782, American Society for Testing and Materials, 1982, p. 1073.
[9] D.R. Olander, Fundamental Aspects of Nuclear Reactor Fuel Elements, Energy Research and Development Administration, TID-26711-P1, 1976, p. 361.
[10] J. Rest, G.L. Hofman, J. Nucl. Mater. 277 (2000) 231.
[11] H. Matzke, Adv. Ceram. 17 (1986) 1.
[12] M.O Marlowe, J. Nucl. Mater. 33 (1968) 242.
[13] K. Nogita, K. Une, Nucl. Instrum. and Meth. B 91 (1994) 301.
[14] J. Spino, D. Papaioannou, J. Nucl. Mater. 281 (2000) 146.
[15] I.L.F. Ray, Hj. Matzke, H.A. Thiele, M. Kinoshita, J. Nucl. Mater. 245 (1997) 115.
[16] M. Kinoshita, T. Kameyama, S. Kitajima, Hj. Matzke, J. Nucl. Mater. 252 (1998) 71.
[17] J. Spino, A.S. Stalios, H. Santa Cruz, D. Baron, J. Nucl. Mater, submitted for publication.
[18] C. Bagger, M. Mogensen, C.T. Walker, J. Nucl. Mater. 211 (1994) 11.
[19] J. Spino, K. Vennix, M. Coquerelle, J. Nucl. Mater. 231 (1996) 179.
[20] Mitchell K. Meyer, Gerard L. Hofman, 'Properties of U–Mo alloy dispersion fuel,' presented at the IAEA Technical Committee on the Development of High Density Uranium–Molybdenum Dispersion Fuels, Vienna, Austria, 23–25 June 2003.
[21] G.L. Hofman, private communication, Argonne National Laboratory, June, 2005.
[22] T. Sonoda, M. Kinoshita, I.L.F. Ray, T. Wiss, H. Thiele, D. Pellotiero, V.V. Rondinella, Hj. Matzke, Nucl. Instrum. and Meth. B 191 (2002) 622.
[23] L.E. Thomas, C.E. Beyer, L.A. Charlot, J. Nucl. Mater. 188 (1992) 80.
[24] K. Nogita, K. Une, J. Nucl. Mater. 226 (1995) 302.
[25] I.L.F. Ray, H. Theile, Hj. Matzke, J. Nucl. Mater. 188 (1992) 90.
[26] J. Spino, J. Rest, W. Goll, T. Walker, J. Nucl. Mater 346 (2005) 226.